

THE INFLUENCE OF CAPILLARY ENTRY-PRESSURE REPRESENTATION ON THE RATE OF CO₂ SOLUBILITY TRAPPING

Boxiao Li, Hamdi A. Tchelepi, and Sally M. Benson

Department of Energy Resources Engineering, Stanford University
367 Panama St, Rm 65, Stanford, CA, 94305, USA
e-mail: boxiaoli@stanford.edu

ABSTRACT

The typical shape of a capillary pressure (P_c) curve is either convex (e.g., Brooks-Corey model) or S-shaped (e.g., van Genuchten model). The Brooks-Corey-type (BC-type) model uses a plateau that ends with a nonzero capillary entry pressure, while the van Genuchten-type (VG-type) model uses a steep slope that connects the end-point (usually zero) to the plateau region. If the slope is steep enough, the two models yield similar simulation results when CO₂ dissolution is not modeled. However, we show that the VG-type model accelerates CO₂ solubility trapping significantly, even when the slope is steep. For long times, the amount of dissolved CO₂ when a VG-type model is used can be twice as large as that obtained when a BC-type model is used.

INTRODUCTION

The dissolution of the CO₂ in the formation water, also known as CO₂ solubility trapping, is an important CO₂ trapping mechanism in the post-injection period of CO₂ sequestration (CCS) in deep aquifers. Modeling solubility trapping requires accurate description of CO₂ plume migration and saturation distribution. Capillary pressure (P_c) is one of the major driving forces of fluid migration in CCS, especially during the post-injection period. Therefore, an accurate representation of the P_c is crucial for modeling solubility trapping, and hence long-term CCS.

Usually, a P_c curve is either S-shaped (e.g., van Genuchten model) or convex (e.g., Brooks-Corey model), as illustrated in Figures 1(a) and (b) (Brooks and Corey, 1964; van Genuchten, 1980). The two models represent the entry of the nonwetting phase into the porous medium differently. While the Brooks-Corey model uses a plateau that ends with a nonzero capillary

entry pressure, the van Genuchten model uses a steep slope that connects the end-point (usually zero) to the plateau region. We name the region around the end-point in VG-type models the “entry slope” region. The height of this region is the pressure difference between the plateau and the end-point, and its width is given by a “threshold” nonwetting-phase saturation, S_{nt} , as illustrated in Figure 1(a). We refer to the entry-pressure representation in Figure 1(a) as a “van-Genuchten-type” (VG-type), and that in Figure 1(b) as a “Brooks-Corey-type” (BC-type). Note that in the VG-type model, the $P_c(S_w = 1)$ can be zero as in Figure 1(a), or nonzero.

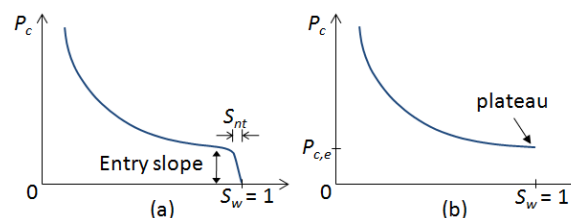


Figure 1. Capillary entry-pressure representations: (a) van-Genuchten-type (VG-type) representation; (b) Brooks-Corey-type (BC-type) representation.

The capillary pressure curves measured in the laboratory using mercury porosimetry usually have an “entry slope” region similar to Figure 1(a), though $P_c(S_w = 1)$ is usually nonzero. There has been wide discussion in the literature on the physical meaning and importance of the entry slope (Schowalter, 1979; Katz and Thompson, 1986; Nabawy et al., 2009). A consensus, however, has not been reached about whether the entry slope should be ignored or honored when interpreting the measurement results. Ignoring the entry slope amounts to applying a BC-type representation, while preserving it amounts to a VG-type representation.

We will show in this work that the representation of the capillary entry pressure can

affect the rate of CO₂ solubility trapping significantly, even when the S_{ni} is very small. Many authors have simulated CCS and performed sensitivity analysis (Ennis-King and Paterson, 2002; Doughty and Pruess, 2004; Pruess and Nordbotten, 2011; Class et al., 2009; Kumar et al., 2005). To our knowledge, the sensitivity of solubility trapping to the representation of the entry pressure (i.e., VG-type versus BC-type curves) has not been investigated. We note that the van Genuchten model has been almost exclusively used in the simulations performed by TOUGH2, a simulator widely used in modeling CCS (Pruess et al. 1999), although several capillary pressure options are available therein. Analytical approaches and high-resolution simulations have been used to model the density-driven convective mixing, which is an important process in solubility trapping (Ennis-King and Paterson, 2005; Riaz et al., 2006; Pruess and Zhang, 2008; Pau et al., 2010; Neufeld et al., 2010). To our knowledge, in most of these and related works, P_c is neglected. Here, we study the impact of the capillary pressure on solubility trapping, with particular emphasis on the representation of the entry-pressure region.

SIMULATION MODEL DESCRIPTION

The aquifer model used in this study is a 2D vertical cross section (x and z directions) of the model proposed by Dahle et al. (2009), which is used as a benchmark for long-term CCS simulations. The 2D model is illustrated in Figure 2, where the size of the aquifer and the location of the injection well are also marked. The aquifer has a dip of 1%, and is deep enough such that the injected CO₂ is in supercritical phase, which is immiscible with the resident water. The top and bottom boundaries are no-flow boundaries. The initial *in situ* pressures at the left and right boundaries are held constant throughout the entire simulation period. Grid size is shown in Table 1. The drainage relative permeability (k_{ri} , $i = w, n$) and P_c curves provided in the benchmark model are used here:

$$k_{rw} = (S_w^*)^4, \quad k_{rn} = 0.4[1 - (\hat{S}_w)^2](1 - \hat{S}_w)^2, \quad (1a)$$

$$S_w^* = (S_w - S_{wi}) / (1 - S_{wi}), \quad S_{wi} = 0.2, \quad (1b)$$

$$\hat{S}_w = (S_w - S_{wi}) / (1 - S_{wi} - S_{nc}), \quad S_{nc} = 0. \quad (1c)$$

$$P_c = P_{c,e} (S_w^*)^{-0.5}, \quad P_{c,e} = 0.2 \text{ bar}. \quad (2)$$

Subscripts w and n denote the wetting (water) and nonwetting (CO₂) phases, respectively. The capillary pressure curve is BC-type, with irreducible water saturation (S_{wi}) as 0.2 and capillary entry pressure ($P_{c,e}$) 0.2 bar. Notice that the critical gas saturation (S_{nc}) in the relative permeability curves is assumed to be zero. Rock properties, salinity, and the depth of the injection well are the same as those in the benchmark model, which are summarized in Table 1.

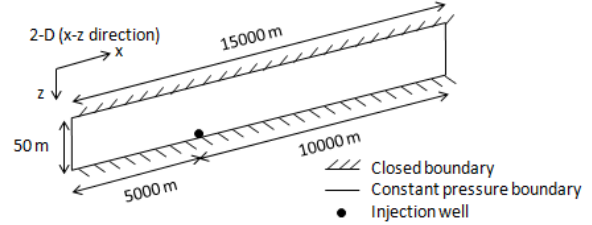


Figure 2. Sketch of the aquifer model.

Table 1: Properties of the aquifer model.

Name	Value
Grid number	$N_x = 150, N_y = 1, N_z = 40$
Gridblock size	$d_x = d_y = 100 \text{ m}, d_z = 1.25 \text{ m}$
Permeability	$k_x = k_y = k_z = 100 \text{ md}$
Porosity	$\phi = 0.15$
Depth at the well	3025 m
Temperature	84.4 °C
Salinity	0

The aquifer is initially fully saturated with water under hydrostatic equilibrium. Pure CO₂ is injected from the well at a rate of 9000 metric tons per year. The injection lasts for 20 years before the well is shut. The simulated time period is 5000 years. All the simulations in this study were performed using an Equation of State (EOS) based compositional simulator, namely, the Stanford General Purpose Research Simulator (GPRS) (Cao, 2002; Jiang, 2007). We did not use TOUGH2 due to difficulties in using different entry-pressure representations for the capillary pressure curves. Detailed EOS tuning parameters for CO₂-water system can be found in Kumar (2004). The Fully Implicit Method (FIM) was used in all the simulations. All the simulations shown here do not account for hysteresis in either capillary pressure or relative permeability curves. We have performed simulations accounting for hysteresis, and have confirmed that our conclusions will not be altered.

SIMULATION RESULTS

Base Case

The base-case simulation uses the VG-type representation (Figure 1a) to modify the P_c curve (Equation 2). Thus, the Brooks-Corey curve is turned into an S-shape curve with $P_c(S_w = 1)$ of zero. The S_{nt} is set as 0.005.

Figure 3 illustrates the distributions of the CO_2 saturation (S_n) and the mole fraction of CO_2 in the aqueous phase (x_{CO_2}) over time. Because it is lighter than water, the injected supercritical CO_2 rises to the top of the aquifer and migrates upward and to the right (the dip is not shown in the figure). As CO_2 dissolves into the water, the plume gets thinner and completely disappears, eventually. The density of the brine increases as more CO_2 dissolves in it. This ultimately leads to the heavier water sinking downward and displacing the lighter CO_2 -free water. Such displacement is unstable, which results in the fingering distribution of the x_{CO_2} .

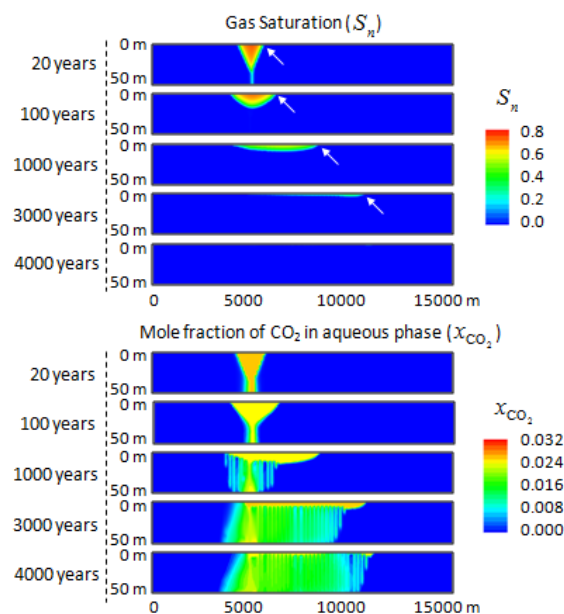


Figure 3. Base-case simulation results: S_n and x_{CO_2} distributions over time. The white arrows indicate the locations of the plume tip. Hysteresis is not simulated for simplicity.

Different Entry-Pressure Representations

Keeping all other parameters unchanged, we conduct simulations using different representations of the capillary entry pressure, as shown in Figure 4. The curve labeled ‘BC-type’ is the

original Equation 2. The curves ‘ $S_{nt} = 0.005$ ’ and ‘ $S_{nt} = 0.0005$ ’ apply the ‘VG-type representation’ based on Equation 2 with their corresponding S_{nt} values. The ‘Silin’ curve is a P_c model from Equation A.1 of Silin et al. (2009), where the fitting parameters $A = B = 0.2$ bar, $\lambda_1 = 0.5$, and $\lambda_2 = 9$. This model is similar to the van Genuchten model, but it has a steeper ‘entry slope.’ All four curves in Figure 4 are similar, except for the small difference near $S_w = 1$. We have also confirmed that the capillary ‘diffusion’ terms for the four cases, defined as

$$D = \frac{\lambda_w \lambda_n}{\lambda_w + \lambda_n} \left| \frac{dP_c}{dS_w} \right|$$

(the phase mobility $\lambda_i = k_{ri} / \mu_i$, $i = w, n$), are bounded. Severe numerical difficulties would occur if D were not bounded.

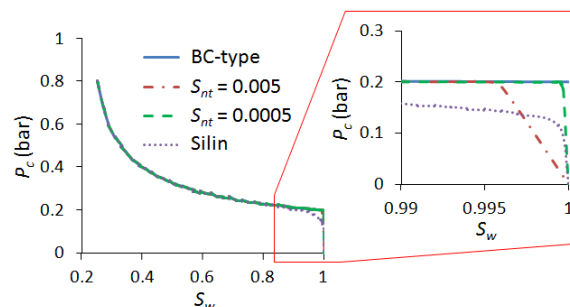


Figure 4. Different representations of the capillary entry pressure.

These apparently small differences in the P_c curves lead to very large differences in the long-term predictions. Figures 5(a) and (b) plot the travel distance of the plume tip and the plume volume for different times. While the ‘ $S_{nt} = 0.005$ ’ case suggests complete dissolution of the CO_2 plume occurring at about 4000 years, only half of the injected CO_2 has dissolved for the ‘BC-type’ case. In addition, the simulation results are sensitive to the steepness of the ‘entry slope’. The plume disappearance is fastest for the Silin case, and slowest for the BC-type case. Such strong sensitivity of the long-term simulation results to the capillary entry-pressure representation is also observed using other industrial reservoir simulators. We note that the sensitivity is not obvious during the injection period, but will intensify and become quite important in the long-term post-injection period.

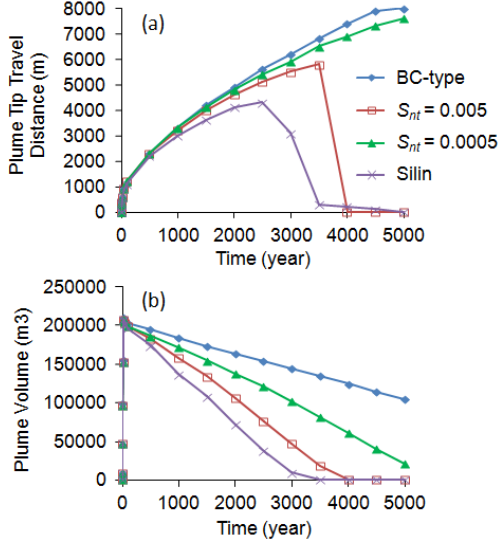


Figure 5. The sensitivity of simulation results to different entry-pressure representations: (a) Distance that plume tip traveled vs. time; (b) Plume volume vs. time.

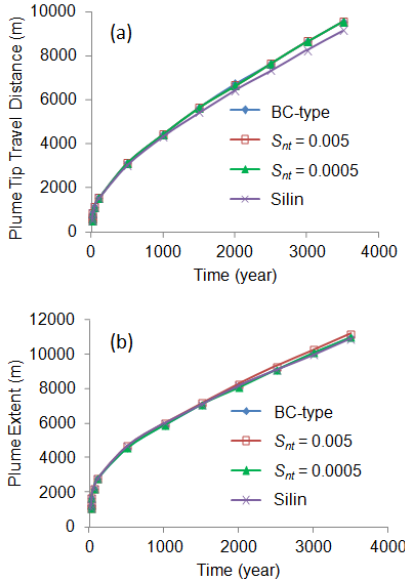


Figure 6. Simulation results for different capillary entry-pressure representations when dissolution is not modeled: (a) Distance that plume tip traveled vs. time; (b) Plume extent vs. time.

Note that although differences in the fluid pressure due to using different capillary entry-pressure representations are present, such differences (0.2 bar at most) are negligible compared with the overall fluid pressure level (about 300 bar), and they are very unlikely to affect the thermodynamic properties of the CO₂ and water, including CO₂ solubility in water.

Note that such sensitivity to the entry-pressure representation is not observed when dissolution is not modeled. Figures 6(a) and (b) show the travel distance and the extent (measured from tail to tip) of the CO₂ plume, if CO₂ is not allowed to dissolve in water. The simulation is terminated when the CO₂ plume reaches the right boundary. As illustrated by the figures, the capillary entry-pressure representation has almost no impact on the results when dissolution is not modeled.

DISCUSSION

Gravity-Capillary-Equilibrium

Due to buoyancy, the injected CO₂ flows towards the top of the porous formation, and accumulates beneath the impermeable cap rock. The column height of the CO₂ plume and the saturation within the plume depend on the interaction between buoyancy and capillary forces. The pressures of the CO₂ and water and P_c can be written as:

$$P_w(z) = P_w|_{z=h_c} - \rho_w g(h_c - z), \quad (3a)$$

$$P_n(z) = P_n|_{z=h_c} - \rho_n g(h_c - z), \quad (3b)$$

$$P_c(z) = P_n(z) - P_w(z), \quad (3c)$$

where z is the depth measured positive downward from the top of the storage formation, and h_c is the column height. Knowing $P_c(z)$ from Equation 3 and the capillary-pressure-saturation relationship, we can compute the CO₂ saturation distribution in the plume column under gravity-capillary-equilibrium analytically as a function of depth, if the total amount of CO₂ in the plume

column, $V = \int_0^{h_c} S_n(z) dz$, is given.

Analytical results and high-resolution numerical simulations were performed using different representations of the capillary entry pressure. Two P_c curves, namely, the ‘ $S_{nt} = 0.005$ ’ and the ‘BC-type’ cases in Figure 4, are compared. The CO₂ and water densities are $\rho_n = 727 \text{ kg/m}^3$ and $\rho_w = 982 \text{ kg/m}^3$, and the viscosities are $\mu_n = 0.070 \text{ cP}$ and $\mu_w = 0.342 \text{ cP}$, respectively, all evaluated at the formation pressure and temperature described earlier. The total amount of CO₂ in the plume column, V , is fixed as 0.64 m. The simulation domain is a 1D vertical column of 50 m, with each gridblock being 5

mm in size, for which numerical diffusion effects are negligible. The permeability k_z is 100 md, the porosity is 0.15, and the relative permeability curves are defined in Equation 1. The top boundary is impermeable, and the initial *in situ* pressure at the bottom boundary is held constant throughout the simulation. Initially, the CO₂ saturation at the top 0.8 m of the domain is $S_n = 1 - S_{wi} = 0.8$ (such that $V = 0.64$ m), below which $S_n = 0$. This corresponds to the sharp-interface assumption that ignores capillary pressure. Since P_c is considered here, the CO₂ column height is expected to expand from the initial condition. The simulation stops when gravity-capillary-equilibrium is reached.

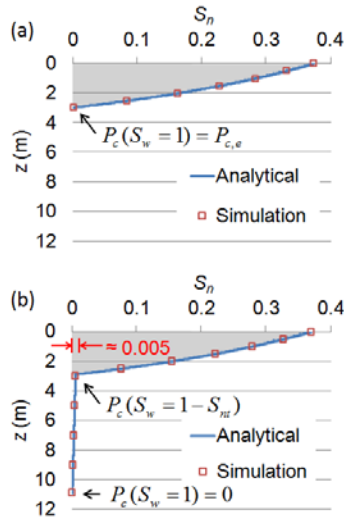


Figure 7. CO₂ saturation distribution within the plume column under gravity-capillary-equilibrium: (a) ‘BC-type’ case; (b) ‘ $S_{nt} = 0.005$ ’ case. The shaded area is the major body of the CO₂ plume.

The CO₂ saturation distributions under gravity-capillary-equilibrium for the two entry-pressure representations are shown in Figure 7. The analytical and numerical solutions agree perfectly (dissolution is not considered here). While the column height of the BC-type case is 2.96 m, the column height of the ‘ $S_{nt} = 0.005$ ’ case is 10.91 m. The additional column height is composed of very little CO₂ saturation, because S_{nt} is only 0.005. For simplicity, hereafter we refer to such additional and low-CO₂-saturation column height as a “saturation tail.” This tail only occurs when the P_c curve applies the VG-type representation. When S_{nt} is small, the length of the saturation tail can be approximated by:

$$h_c^{VG} - h_c^{BC} \approx [P_c^{BC} |_{S_w=1} - P_c^{VG} |_{S_w=1}] / [(\rho_w - \rho_n)g], \quad (4)$$

where the superscripts BC denotes BC-type representation, and VG denotes VG-type representation. If $P_c(S_w = 1)$ for the VG-type representation is zero, which is the case in previous examples, the right hand side of Equation 4 becomes $P_c^{BC} |_{S_w=1} / [(\rho_w - \rho_n)g]$.

As long as the major CO₂ body has enough CO₂ to supply the saturation tail, the length of the tail is not influenced by the thickness of the major body. Because the tail is composed of very little saturation, it can form even if the major body of the CO₂ plume is thin. The tail is longer when the density contrast between water and supercritical CO₂ is low, which is usually the case in deep storage formations. The influence of the tail becomes increasingly evident as the CO₂ plume migrates under the cap rock and becomes stretched and thinner with time. We reiterate that the saturation tail is not an artifact of numerical diffusion—it is corroborated by analytical calculation and fine-grid simulation. Although the total column heights for the two cases are dramatically different, the CO₂ saturation in the saturation tail is so small that it almost makes no impact in simulations that do not account for dissolution, and it does not affect the extent and the migration speed of the CO₂ plume. Figure 6 illustrates this point.

However, for long-term CCS simulations, where CO₂ dissolution is included, the CO₂ delivered to the long saturation tail will quickly dissolve in water. The tendency toward gravity-capillary-equilibrium keeps delivering CO₂ to sustain the tail, until the water surrounding the tail is fully saturated by the dissolved CO₂. Figure 8 illustrates the evolution of the CO₂ column height subject to dissolution. The CO₂ solubility (expressed as mole fraction, x_{CO_2}) is 0.0254. All other properties, model grid, and the boundary conditions are unchanged. The initial condition is the same sharp-interface condition as earlier, where the water in the initial two-phase region is fully saturated with dissolved CO₂. The amount of the dissolved CO₂ is characterized by the parameter $X = \int_0^{h_c} x_{CO_2}(z) dz$. As indicated in Figure 8, the growth of the saturation tail is hindered by CO₂ dissolution, but the tendency is

to keep transferring CO₂ from the major CO₂ body to the underlying water, causing more CO₂ to be dissolved. Eventually, the amounts of dissolved CO₂ for the two cases become significantly different. So far, all of the simulations covered in this section have been in 1D, where the convective mixing of CO₂ and water—a multidimensional process—is suppressed. Discussion on convective mixing is covered in the next subsection.

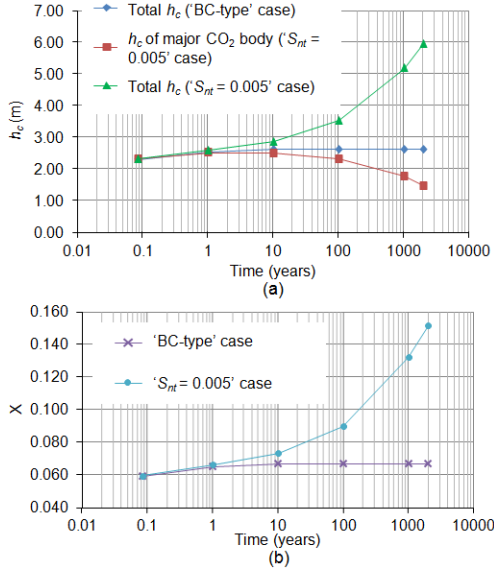


Figure 8. Development of the capillary transition zone for different entry-pressure representations (dissolution is modeled): (a) column height (h_c); (b) amount of dissolved CO₂ (X).

The saturation tail is essentially part of the capillary transition zone. The characteristic time scale for the development of the transition zone can be derived as (Nordbotten and Dahle, 2008):

$$t^* = \frac{\phi}{k_z (\Delta\rho g)^2} \left(\frac{1}{\lambda_w} + \frac{1}{\lambda_n} \right)^* \left(\frac{dP_c}{dS_w} \right)^*, \quad (5)$$

where the superscript * denotes characteristic values. As indicated by Equation 5, the lower the density contrast between water and CO₂, the longer the time for the transition zone, and hence the saturation tail, to develop—but eventually the tail length will be larger (also see Equation 4). In addition, large vertical permeability of the storage formation and large CO₂ mobility facilitate the development of the ‘saturation tail’. An important element in the CO₂ relative permeability curve is the critical CO₂ saturation (S_{nc} , see Equation 1). It is defined as the

minimum CO₂ saturation that allows the CO₂ to flow in the porous medium for a drainage process. The CO₂ is mobile only if its saturation is above S_{nc} . If S_{nc} is larger than S_{nt} (width of the ‘entry slope’, see Figure 1a), the saturation tail will not form, due to zero mobility of the CO₂. However, laboratory measurements of CO₂-water drainage relative permeability curves suggest that S_{nc} can be close to zero (Bennion and Bachu, 2006; Perrin and Benson, 2008). It is difficult, in practice, to measure the S_{nc} in a typical core flood experiment accurately. More importantly, the CO₂ relative permeability at $S_n = S_{nt} = 0.005$ is only $O(10^{-7})$ (as calculated from Equation 1) in the simulations described above, where $S_{nc} = 0$. However, even with very low CO₂ mobility, the saturation tail can still grow and influence long-term simulation results dramatically. Therefore, when the VG-type representation is applied to the P_c curve, the simulation result is very sensitive to the value of S_{nc} .

Density-Driven Convection

In multiple dimensions, convective mixing of the heavier CO₂-rich and the lighter CO₂-free water is expected to take place, and the mixing behavior can be influenced by the presence or absence of a saturation tail.

Although many authors have analyzed and modeled the convective mixing problem (Ennis-King and Paterson, 2005; Riaz et al., 2006; Pruess and Zhang, 2008; Pau et al., 2010; Neufeld et al., 2010), to our knowledge, P_c is neglected in most of these and related works. This simplification allows one to analyze or simulate only the single-phase (CO₂-rich and CO₂ free water) region. However, in many cases, the capillary transition zone cannot be ignored, and the two-phase behavior must be carefully studied.

Here, fine-grid, 2D, two-phase numerical simulations were performed to investigate the effect of the entry-pressure representation. The porous medium is 10 m × 50 m in the x and z directions, and each gridblock is 0.1 m × 0.2 m. All the properties, initial conditions, and top and bottom boundary conditions are the same as the simulations that produce Figure 8. The left and right boundaries are periodic, which amounts to

rolling up the domain about a vertical axis and connecting the left boundary to the right. Different entry-pressure representations are employed based on Equation 2. The simulation results are compared in Figure 9, which shows the development of convective fingers after 10 years. The VG-type representation clearly yields more CO₂ dissolution than the BC-type representation. Figure 9 is produced using a first-order two-phase simulator, and it provides merely a rough qualitative comparison. However, this is adequate to demonstrate the importance of the entry-pressure representation on convective mixing. In addition, results from many other such simulations we have performed support our observations. Performing high-order multiphase simulations is exceptionally challenging, and to our knowledge, all of the high-order simulations in the literature that model the convective mixing are for miscible single-phase flow.

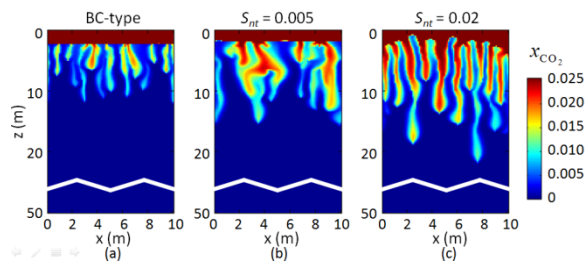


Figure 9. Impact of different entry-pressure representations: (a) BC-type representation; (b) VG-type representation, $S_{nc} = 0.005$; (c) VG-type representation, $S_{nc} = 0.02$.

CONCLUDING REMARKS

The typical shape of a capillary pressure curve is either convex (e.g., Brooks-Corey model) or S-shaped (e.g., van Genuchten model). Both models are widely used in simulating long-term CCS. The Brooks-Corey-type (BC-type) model uses a plateau to represent the nonwetting-phase entry into the porous medium, while the van-Genuchten-type (VG-type) model uses an entry slope, which connects the end-point to the plateau region. In this paper, we simulate long-term CCS using these two representations of the capillary entry pressure, and we assign a steep entry slope to the VG-type model to reduce the difference between the two representations. Although the two entry-pressure representations produce similar results when CO₂ dissolution is

ignored, the simulation results are dramatically different in the long-term post-injection period if dissolution is modeled. The entry slope of the VG-type capillary pressure curve tends to create a longer CO₂ column height due to the interactions of gravity and capillary forces. High-resolution simulations have confirmed that this is not a numerical artifact. The additional column height consists of very small CO₂ saturation, which can dissolve quickly into the surrounding water. The tendency toward gravity-capillary-equilibrium keeps transferring more CO₂ from the major CO₂ plume body to the underlying water through this additional column height. Density-driven convection then carries the CO₂-rich water away and brings CO₂-free water close by, causing more CO₂ to dissolve. This vertical mass-transfer mechanism introduced by the VG-type representation causes faster CO₂ dissolution compared with the BC-type representation. This is especially the case in deep storage formations where the density contrast between water and CO₂ is low, and in formations that have large vertical permeabilities and small critical CO₂ saturation (S_{nc}) values.

Capillary pressure curves measured in the laboratory tend to have an entry slope region. Consensus has not been reached regarding the importance of this entry slope region. Careful measurements, preferably on core or larger scale, are needed to study this issue. Note that the intention of this work is not to argue whether such entry slope is real in natural systems. The intention is, rather, to point out that the VG-type capillary pressure model, which is widely used in modeling long-term CCS, will cause accelerated CO₂ dissolution, compared with the BC-type model. This has not been reported in the literature. We should also note that the VG-type representation brings several challenges in modeling long-term CCS. First, the simulation results are more sensitive to the steepness of the entry slope and to the S_{nc} value. The S_{nc} can be very small for a CO₂-water system and can be difficult to measure accurately from experiments. Second, the steepness and the curvature introduced by the entry slope challenge the nonlinear solver of the simulator, making the computation highly inefficient. Using a convex capillary pressure model such as a Brooks-Corey model, is computationally

straightforward, and leads to conservative estimates for the amount of CO₂ solubility trapping.

ACKNOWLEDGMENT

The authors acknowledge Dr. Gary Li and Dr. Yaqing Fan for their helpful discussions.

REFERENCES

[1] Brooks, R.H. and A.T. Corey, *Hydraulic Properties of Porous Media*, Colorado State University, Fort Collins, Colo., 1964.

[2] van Genuchten, M.T., A Closed-form Equation for Predicting the Hydraulic Conductivity of Unsaturated Soils, *Soil Sci. Soc. Am. J.*, 44(5), 892-898, 1980.

[3] Schowalter, T.T., Mechanics of Secondary Hydrocarbon Migration and Entrapment, *AAPG Bulletin*, 63(5), 1979.

[4] Katz, A.J. and A.H. Thompson, Quantitative Prediction of Permeability in Porous Rock, *Phys. Rev. B*, 34(11): 8179-8181, 1986.

[5] Nabawy, B.S., et al., Pore-Throat Characterization in Highly Porous and Permeable Sandstones." *AAPG Bulletin*, 93(6): 719-739, 2009.

[6] Ennis-King, J. and L. Paterson, Engineering Aspects of Geological Sequestration of Carbon Dioxide, SPE Asia Pacific Oil and Gas Conference and Exhibition, Melbourne, Australia, 2002.

[7] Doughty, C. and K. Pruess, Modeling Supercritical Carbon Dioxide Injection in Heterogeneous Porous Media, *Vadose Zone J.*, 3(3), 837-847, 2004.

[8] Pruess, K. and J. Nordbotten, Numerical Simulation Studies of the Long-term Evolution of a CO₂ Plume in a Saline Aquifer with a Sloping Caprock, *Transp. Porous Med.*, 90(1), 135-151, 2011.

[9] Class, H., et al., A benchmark study on problems related to CO₂ storage in geologic formations. *Comput. Geosci.*, 13(4), 409-434, 2009.

[10] Kumar, A., et al., Reservoir Simulation of CO₂ Storage in Deep Saline Aquifers. *SPE J.*, 10(3), 336-348, 2005.

[11] Pruess, K., C. Oldenburg, and G. Moridis, *TOUGH2 User's Guide, Version 2.0*, Report LBNL-43134, Lawrence Berkeley National Laboratory, Berkeley, Calif., 1999.

[12] Ennis-King, J. and L. Paterson, Role of Convective Mixing in the Long-Term Storage of Carbon Dioxide in Deep Saline Formations, *SPE J.*, 10(3): 349-356, 2005.

[13] Riaz, A., et al., Onset of Convection in a Gravitationally Unstable Diffusive Boundary Layer in Porous Media, *J. Fluid Mech.*, 548, 87-111, 2006.

[14] Pruess, K. and K. Zhang, Numerical Modeling Studies of the Dissolution-Diffusion-Convection Process During CO₂ Storage in Saline Aquifers, Lawrence Berkeley National Laboratory Report, 2008.

[15] Pau, G.S.H., et al., High-Resolution Simulation and Characterization of Density-Driven Flow in CO₂ Storage in Saline Aquifers, *Adv. Water Resour.*, 33(4), 443-455, 2010.

[16] Neufeld, J.A., et al., Convective Dissolution of Carbon Dioxide in Saline Aquifers, *Geophys. Res. Lett.*, 37(22), L22404, 2010.

[17] Dahle, H.K., et al. A Model-Oriented Benchmark Problem for CO₂ Storage, 2009; http://org.uib.no/cipr/Workshop/2009/CO2/benchmark_definition.pdf.

[18] Cao, H., *Development of Techniques for General Purpose Simulators*, Ph.D. Thesis, Stanford University, 2002.

[19] Jiang Y., *Techniques for Modeling Complex Reservoirs and Advanced Wells*, Ph.D. Thesis, Stanford University, 2007.

[20] Kumar, A., *A Simulation Study of Carbon Sequestration in Deep Saline Aquifers*, M.S. Thesis, University of Texas at Austin, 2004.

[21] Nordbotten, J. M. and H.K. Dahle, Impact of the Capillary Fringe in Vertically Integrated Models for CO₂ Storage, *Water Resour. Res.*, 47(2), W02537, 2011.

[22] Bennion, D.B. and S. Bachu, Dependence on Temperature, Pressure, and Salinity of the IFT and Relative Permeability Displacement Characteristics of CO₂ Injected in Deep Saline Aquifers. SPE Annual Technical Conference and Exhibition. San Antonio, Texas, USA, 2006.

[23] Perrin J.C. and S.M. Benson, Relative Permeability Explorer, Benson Lab, Stanford University, 2008. <http://pangea.stanford.edu/research/bensonlab/reperm/index.html>.